innoTRAC Journal
Volume 2 (2022), pp. 69–89
https://doi.org/10.14464/innotrac.v2i1.576

Experimental verification of analytical calculation approaches and FEM material models with the aim of determining friction of thermoplastics

Niels Dallinger[1*], André Bergmann[1], Markus Golder[1], Timo Bensing[2], Martin Moneke[2]

[1] *Professorship of Conveying Engineering and Materials Handling, Chemnitz University of Technology, Germany*
[2] *Institute of Plastics Engineering, Darmstadt University of Applied Sciences, 64295 Darmstadt, Germany*
[*] *Correspondence: niels.dallinger@mb.tu-chemnitz.de; Tel.: +49-371-531-39436*

Received 30 June 2022; Accepted 30 July 2022; Available online 15 December 2022

ABSTRACT The paper presents analytical approaches for calculating the effective contact area of the sphere-plane contact, which allow conclusions to be drawn about the coefficient of friction of thermoplastics with manageable effort. These approaches are verified experimentally utilizing friction and wear tests using the example of a steel sphere against PE-UHMW. The friction area of the sphere was varied using a self-constructed adjustment unit and a spherical wedge. With the help of parametric experiments regarding the angular position of the spherical wedge, a limiting contact angle was detected. This limiting angle allows the calculation of the deformative and adhesive friction. FE models are being developed for the simulative verification of the analytical approaches and further investigations of structures for friction reduction. These require specific material models as a basis for the representation of the stress-strain behavior in contact. The different FEM material models are calibrated and compared against each other based on experimental tests. The materials POM, PP, PMMA, and PE-UHMW were considered.

KEYWORDS friction, thermoplastics, polymer, tribology, wear, simulation, contact

1. Introduction

In order to make friction and wear predictable, the material deformations must first be calculated. The basic approaches for the calculation were described in [1]. Building on this, this article describes the comparison of initial test results with the previously defined calculation approaches.

The Finite Element Method (FEM) material models for the polymers polyoxymethylene (POM), polypropylene (PP) and ultra-high-molecular-weight polyethylene (PE-UHMW) are generated and validated on the basis of fundamental mechanical tests. These include tensile and compression tests, as well as indentation tests of steel spheres into the relevant polymers.

With regard to the analytical model, the calculation approaches from [1] are adapted for the special case of a sphere in contact with a cylindrical groove and compared with lubricated friction experiments.

2. Materials

The polymers investigated in this article are PE-UHMW, POM and PP. These engineering thermoplastics are commonly used in all areas of industry including automotive, materials handling or medical engineering. Besides the advantage of possible low-cost production by injection moulding or extrusion these polymers have self-lubrication properties which enables the tribological use under dry conditions.

PE-UHMW

For this investigation Röchling Polystone® M Natur was used. It is a PE-UHMW without additives and is characterised by its high abrasion and wear resistance, combined with high impact strength. The tensile modulus is 680 MPa. For further information, see [2].

POM

For the material POM a standard injection moulding type, Celanese Hostaform® C 9021 was chosen. This POM-Copolymer is characterised by high rigidity, hardness and toughness. The tensile modulus is 2850 MPa. For further information, see [3].

PP

For PP, a LyondellBasell POLYFORT® FPP 22 T LE K1684 was used. This is a 22% talc filled heat stabilized PP-Homopolymer which is often used in the automotive industry. The tensile modulus is 2600 MPa. For further information, see [4].

Steel-Spheres

For the instrumented indentation tests and the investigation of coefficient of friction (COF) steel spheres made of 1.3505 with a diameter of 8 mm were used. The grade is G20 (according DIN 5401:2002-8).

Silicone oil

For determining the deformative part of COF, μ_{def}, lubricated friction tests were carried out with silicone oil. The viscosity is 50 mm²/s and therefor comparable with water. For further information, see [5].

3. Experimental Setup

3.1. Tensile Tests

In order to calibrate the FEM material model with regard to the tensile properties, the required data were determined by means of uniaxial tensile tests with variation of the test velocity. Figure 1 shows the test setup with a clamped POM specimen.

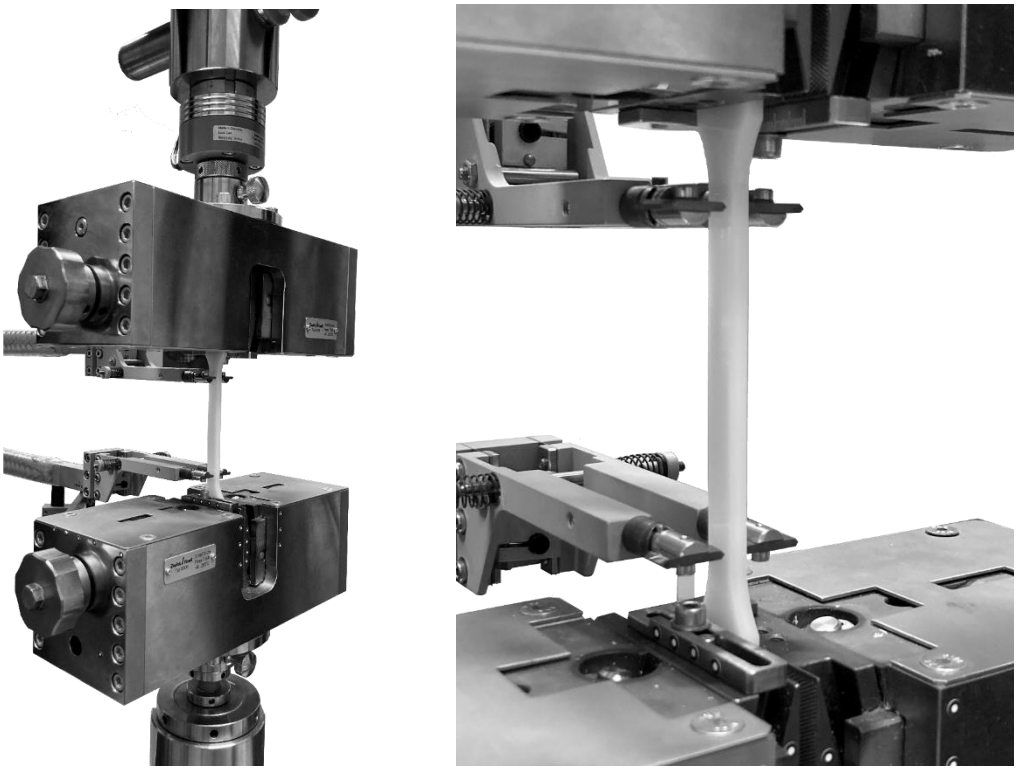

Figure 1: tensile testing machine with external extensometer

Test parameters:

- Machine: Zwick Roell Z100, equipped with external extensometer
- Load cell: 10 kN
- No Preload
- Crosshead velocity: 1, 5, 50, 500 mm/min

Specimen:

- PP and POM: tensile bar type 1A with 115 mm clamping length
- PE-UHMW: rectangular bar (10 x 25 mm) with 115 mm clamping length

number of repetitions:

- PP and POM: 10 tests (except 1 mm/min: 5 tests)
- PE-UHMW: 5 tests

The charts in Figure 2 show a selection of the results from the tensile tests for the respective material until they reach the break-off criterion. The termination criteria of the tensile tests are the breakage of the specimen or the maximum crosshead travel. In

the case of PE-UHMW at a loading velocity of 1 mm/min, the test was manually terminated. For all materials there is a stiffening effect with an increase in velocity.

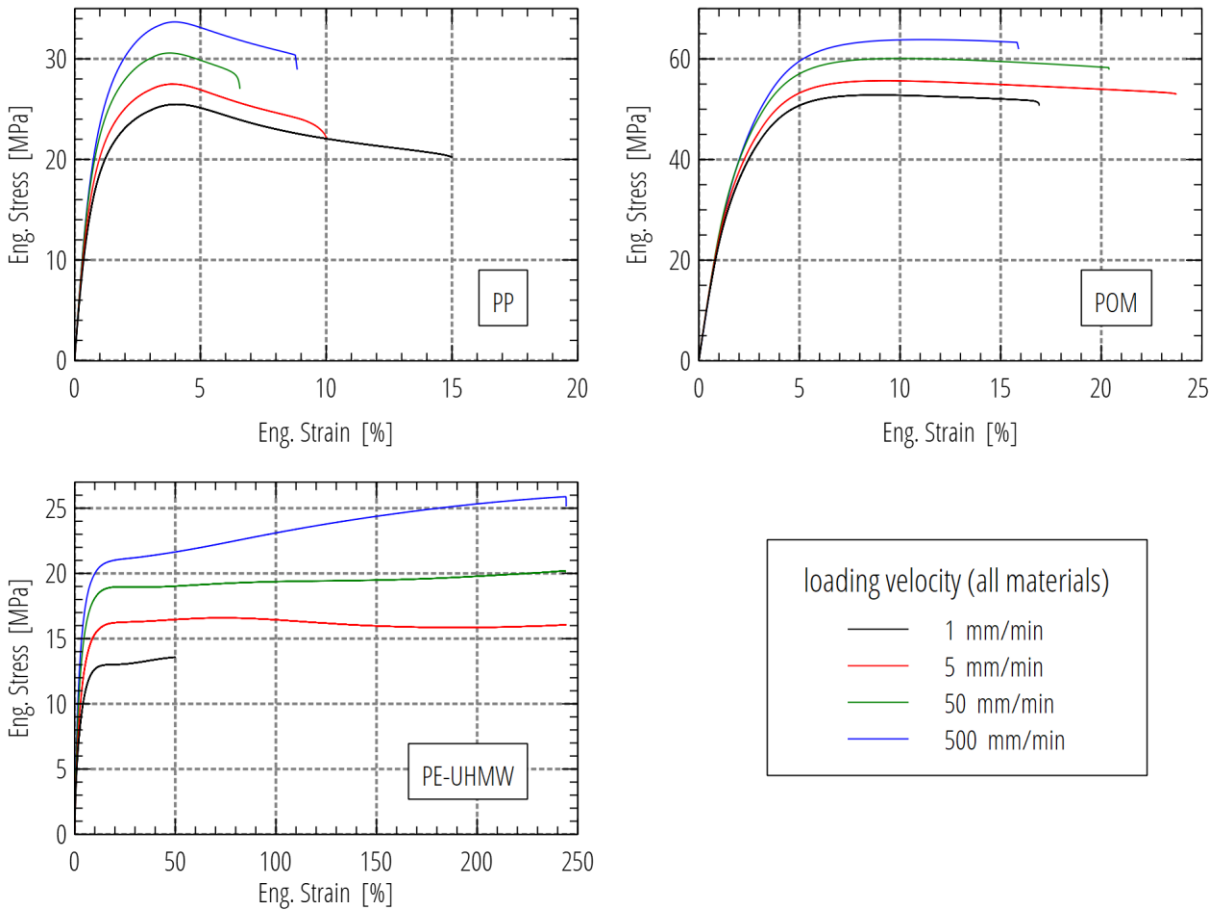

Figure 2: results of selected tensile tests for each material at different loading velocities

3.2. Compression Tests

The required data regarding the compression behaviour of the polymers were determined by compression tests with two different testing velocities. The test setup is shown in Figure 3.

Test parameters:

- Machine: Zwick Roell Z100
- Load cell: 10 kN
- Crosshead velocity: 5, 50 mm/min
- number of repetitions: 5 tests

Specimen:

- PP POM and PEUHMW: rectangular bar with 4x4x20 mm
- PE-UHMW: rectangular bar with 7x7x20 mm and 8x8x20 mm

The graphs in Figure 4 show a selection of the results from the compression tests for the respective material. Again, a stiffening effect occurs with an increase in velocity for all materials. The compression tests were evaluated until they reach the buckling limit

according to [6]. Depending on the dimensions of the specimen, these limits differ. All graphs in Figure 4 show processed measured values. The individual curves were linearized in the initial area. In addition, a zero-point correction was performed afterward.

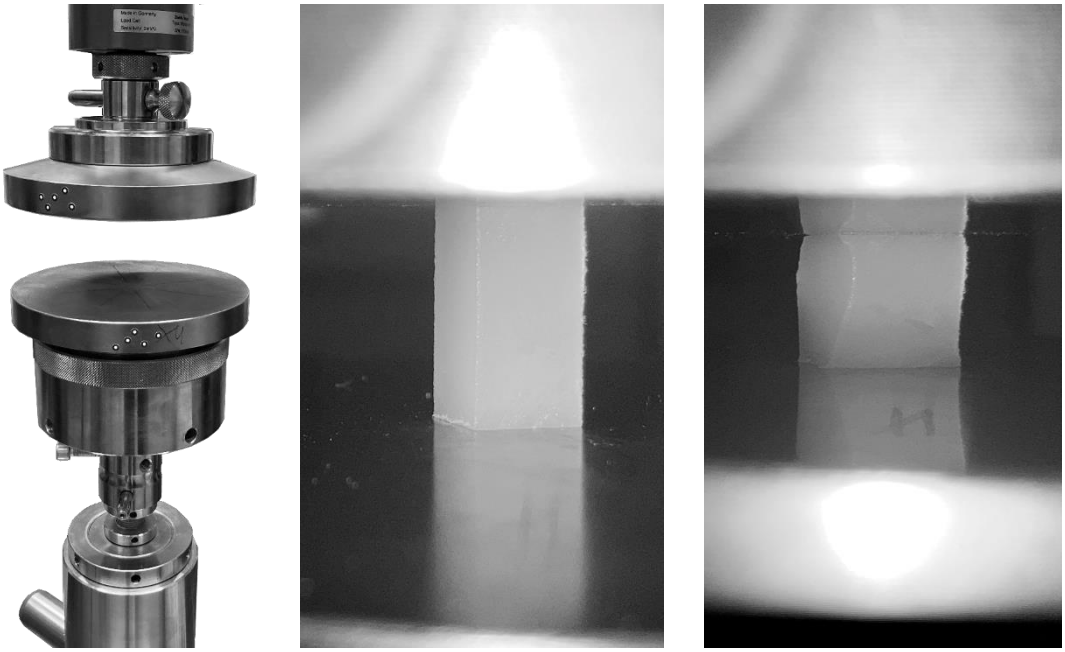

Figure 3: compression testing setup with PE-UHMW specimen

The unprocessed measured values of the compression tests show deviations from the expected material behaviour. These deviations led to the investigation of the possible causes. To classify these anomalies more closely, the influence of various factors within a compression test were examined. To achieve an accurate insight on these effects the FEM was used. A three-dimensional model of a compression specimen between two loading platens allows to variate some fundamental boundaries conditions with low effort.

As the first set of parameters, the contact area and the friction values between the loading platens and the specimen are investigated concerning their influence on the progress of the stress-strain curve. The charts in Figure 5 show the impact regarding a variation of the coefficient of friction.

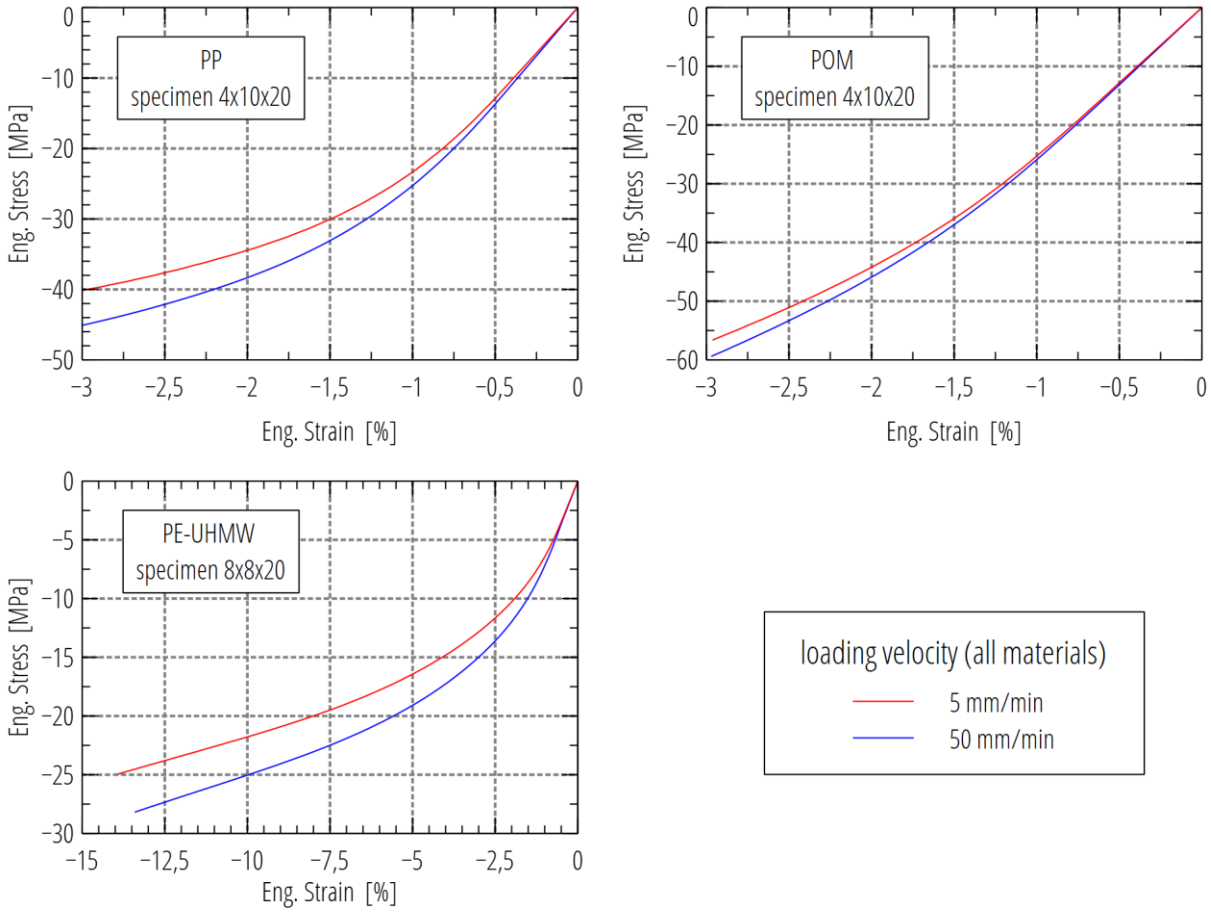

Figure 4: Result of selected compression tests for each material at different loading velocities (specimen dimensions in mm)

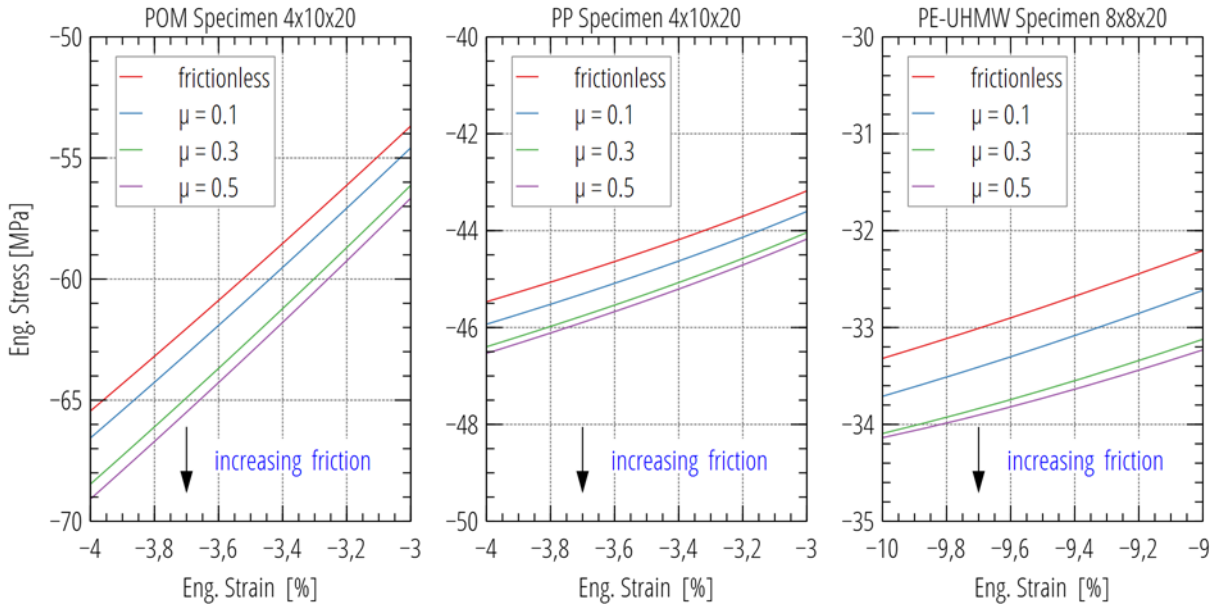

Figure 5: Parametric FEM study; variation of coefficient of friction between specimen and loading platens (specimen dimensions in mm)

According to Figure 6, the effect of the size of contact area on the progress of the stress-strain graphs leads to a clear recommendation for the design of the specimen. Using

specimen with low contact areas is the best choice to minimize the effects of apparently stiffening.

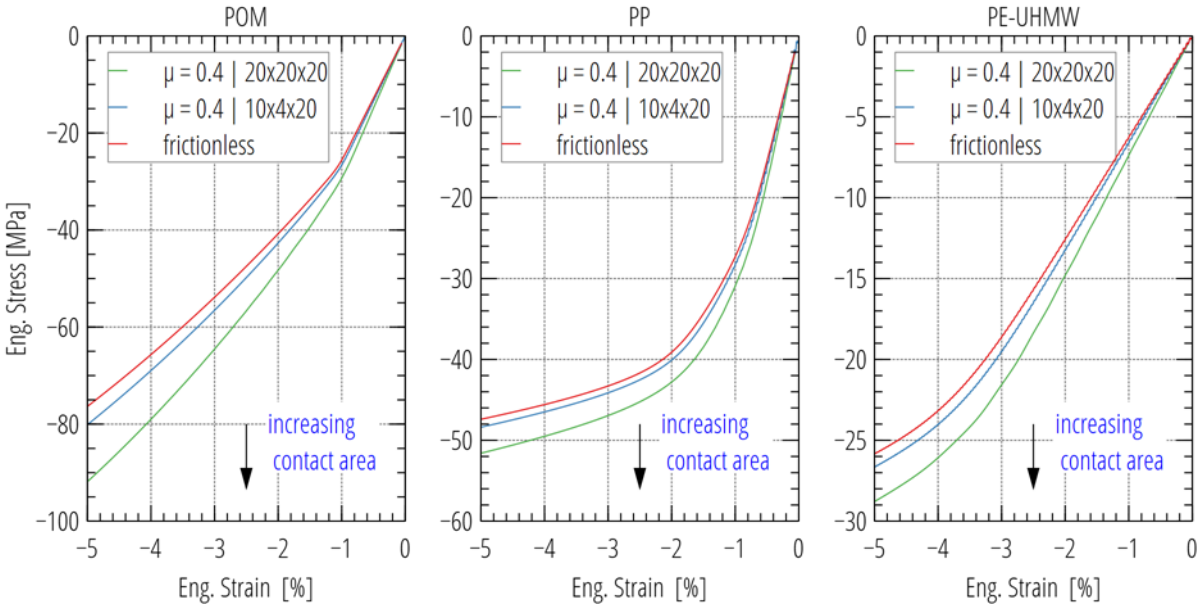

Figure 6: Parametric FEM study; variation of contact area between specimen and loading platens (specimen dimensions in mm)

It could be shown that the effect already described by Bergström in [7] is a relevant parameter in the material analysis. With increasing contact area and increasing coefficient of friction, the deviation from the friction-free reference sample also increases. However, the relative deviation decreases with increasing specimen length. The ratio of contact area to specimen length is therefore decisive for effective specimen design. Nevertheless, the length of the specimen is also the most significant factor in determining the buckling-free compression and limits the evaluable range of measured values.

Another important factor is the parallelism of the loading platens. An inclination of the plates causes an asymmetrical load on the specimen, especially in the initial area of the compression tests, and consequently an over-proportional increase in displacement. The following Figure 7 shows the angular deviations determined on the test setup.

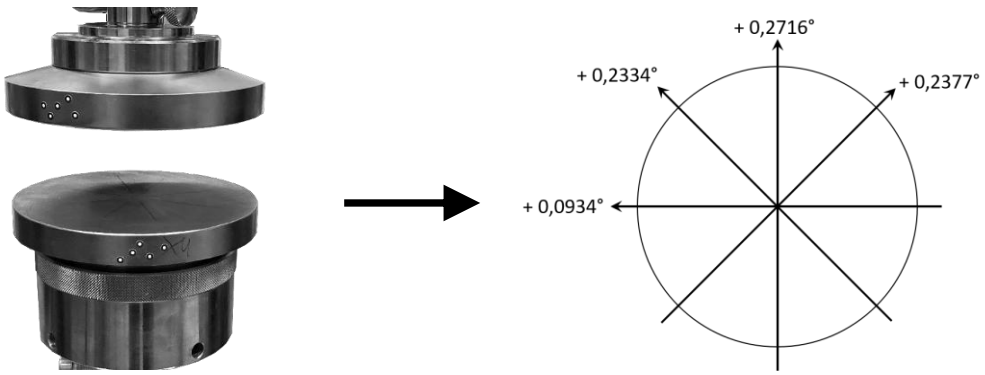

Figure 7: measured angular deviations (deviation of parallelism) between the loading platens at the compression testing setup (top view)

Figure 8 shows the influence of an angular deviation between the two loading platens on the measured stress-strain values. The specimen within the FEM model is absolutely parallel. The simulation investigates the influence of a non-perpendicular compression force on the specimen.

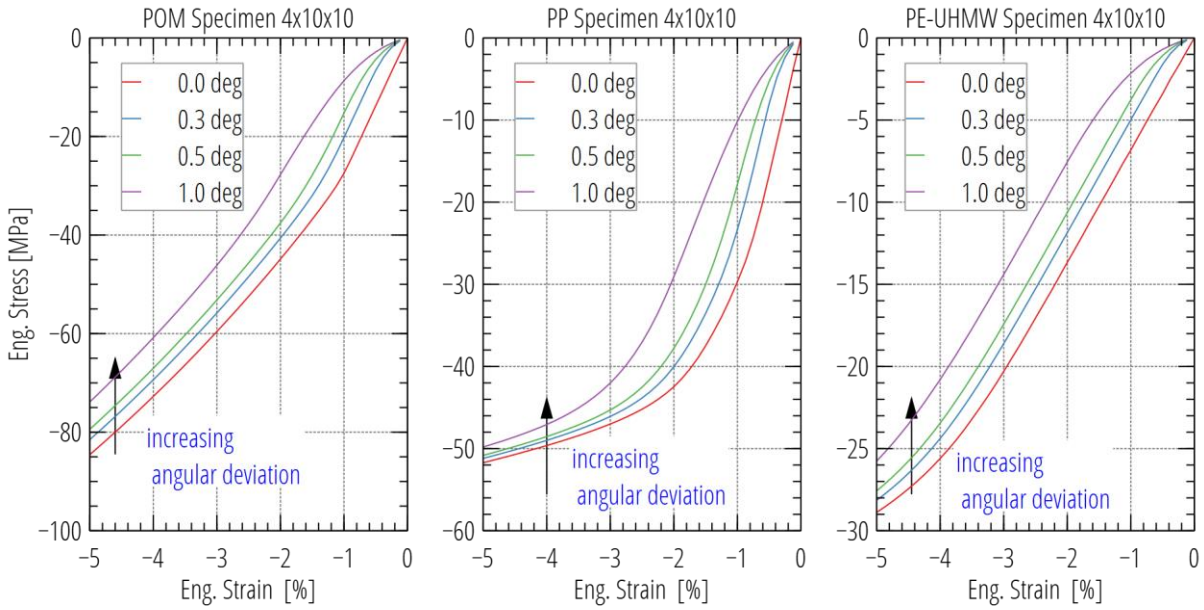

Figure 8: Parametric FEM study; variation angular deviation between the loading platens (specimen dimensions in mm)

The parametric FEM studies give us clear design recommendations to minimize the errors during the evaluation of the compression test. Our goal is to evaluate the widest possible range of strains. This requirement is strongly limited by the buckling susceptibility of the specimen. Table 1 provides an overview of the relationship between specimen geometry and critical compression, which ultimately leads to buckling. It includes the recommendations according to [6] and the selected specimen dimensions.

The specimen for the materials PP and POM have to be taken from tensile bars and therefore are limited to the cross-section of 4 x 10 mm². To minimize the susceptibility to errors concerning friction, a specimen length of 20 mm was chosen. However, this considerably limits the strain that can be evaluated. Test specimen for PE-UHMW can be produced in different dimensions, resulting in a significantly broader buckling-free strain range during evaluation.

Table 1: Overview of the geometries of test specimen for the compression tests

length [mm]	thickness [mm]	width [mm]	buckling limit crit. compression	notes
50	4	10	0.5 %	DIN ISO EN 604 type A
10	4	10	13.2 %	DIN ISO EN 604 type B
20	4	10	3.3 %	Specimen for PP, POM, PE-UHMW
20	8	8	13.2 %	Specimen for PE-UHMW (type 1)
20	7	7	10.1 %	Specimen for PE-UHMW (type 2)

3.3. Instrumented Indentation tests

Beside the mentioned uniaxial tensile and compression tests another test procedure was needed that could cover the complex stress conditions during friction. Therefor instrumented indentation tests were carried out, where a steel indenter (sphere ø 8 mm) is pressed into the polymer with a defined testing velocity and normal load FN. After a certain holding time the normal load is released with the same velocity. The results are used for calibrating the FE material models. Figure 9 (left) shows the test set up with a PE-UHMW specimen and the resulting plastic spherical indentation after the test (right).

Test parameters:

- Machine: Zwick Roell Z250, equipped with external extensometer
- Load cell: 500 N
- Preload: 2 N
- Normal load: 20, 50, 100, 150 N
- Indentation velocity: 1 – 100 N/s

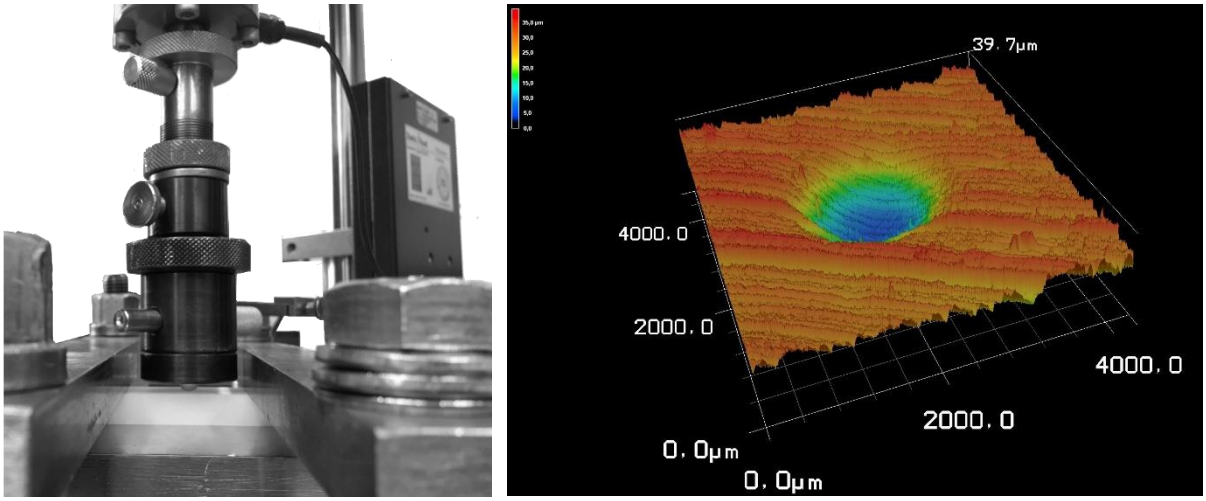

Figure 9: (left): Test set up for indentation tests with external extensometer; (right): plastic deformation after static indentation test with FN = 150 N

As an example Figure 10 shows the test results of the indentation test for PE-UHMW for different normal loads in detail. First, the normal load is applied with 100 N/s and then the particular load is held for 3 s. Within that time all samples are subject to creep. After releasing the load, the evolution of the indentation depth is recorded for 120 s where again creeping occurs.

Since the friction process involves high deformation velocities, these tests should also be carried out with high velocities. However, the limiting factor is the controlling performance of the machine. One negative example is the graph with 20 N normal load, where at the beginning of the test the load is oscillating and no stable indentation depth can be observed.

For the other two materials (POM, PP), which are stiffer, only lower velocities could therefore be investigated. For the lowest load of 20 N a velocity of 20 N/s was used and for all other loads 50 N/s were applied.

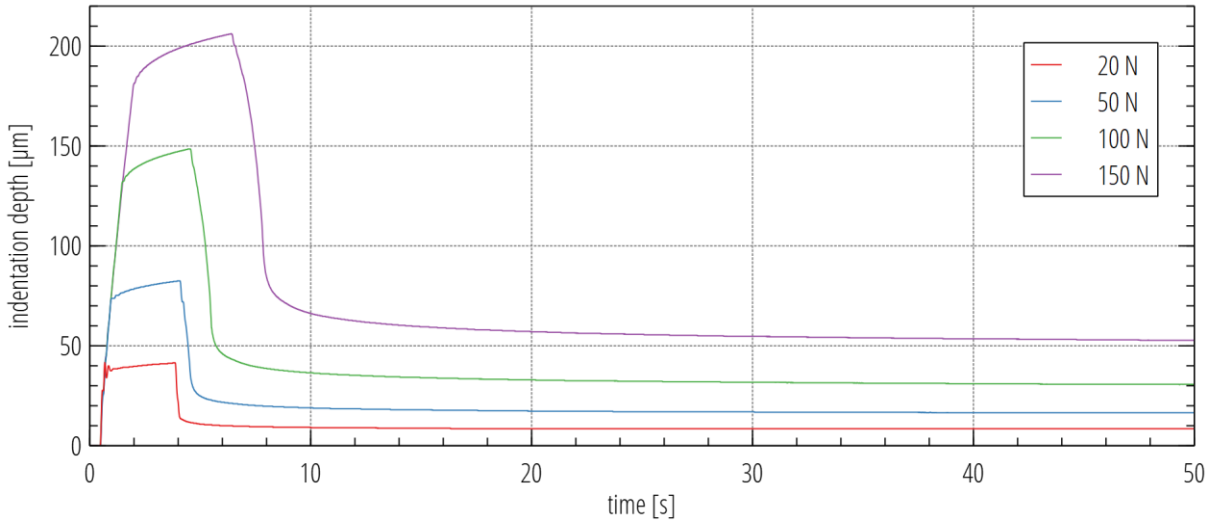

Figure 10: indentation depth over time for PE-UHMW under variation of the normal load; tested with a velocity of 100 N/s; load holding time 3 s; unloading time 120 s (only 50 s are shown)

The summarised results for PE-UHMW, POM and PP are presented in Figure 11. For all materials, the penetration depth is shown directly after the particular load is applied and the remaining depth is shown after a release time of 120 s. The non-linear behaviour is evident.

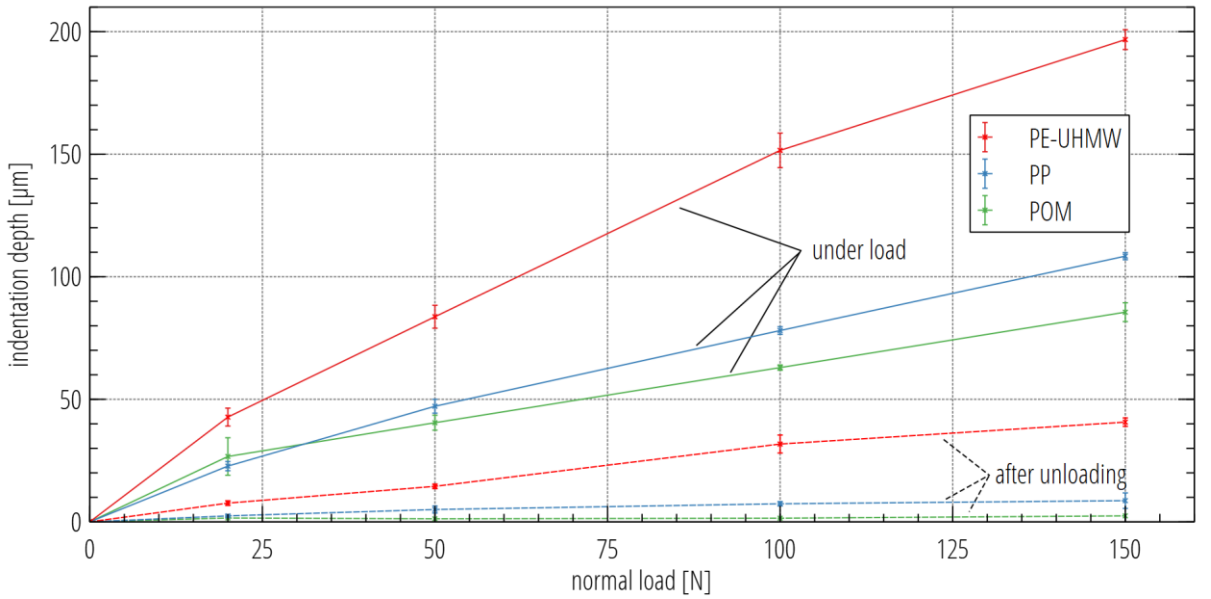

Figure 11: indentation depth over time for PE-UHMW under variation of the normal load; tested with a velocity of 100 N/s; load holding time 3 s; unloading time 120 s (only 50 s are shown)

3.4. Friction Test Machine

To measure friction and the indentation depth (or wear) a ball on disc test machine is used (see Figure 12). During the test, a PE-UHMW disc is rotating and a steel sphere is brought into contact under a defined normal load FN. The testing device enables the measurement of COF, temperature and indentation depth over long time. The tests can be performed in dry and wet conditions.

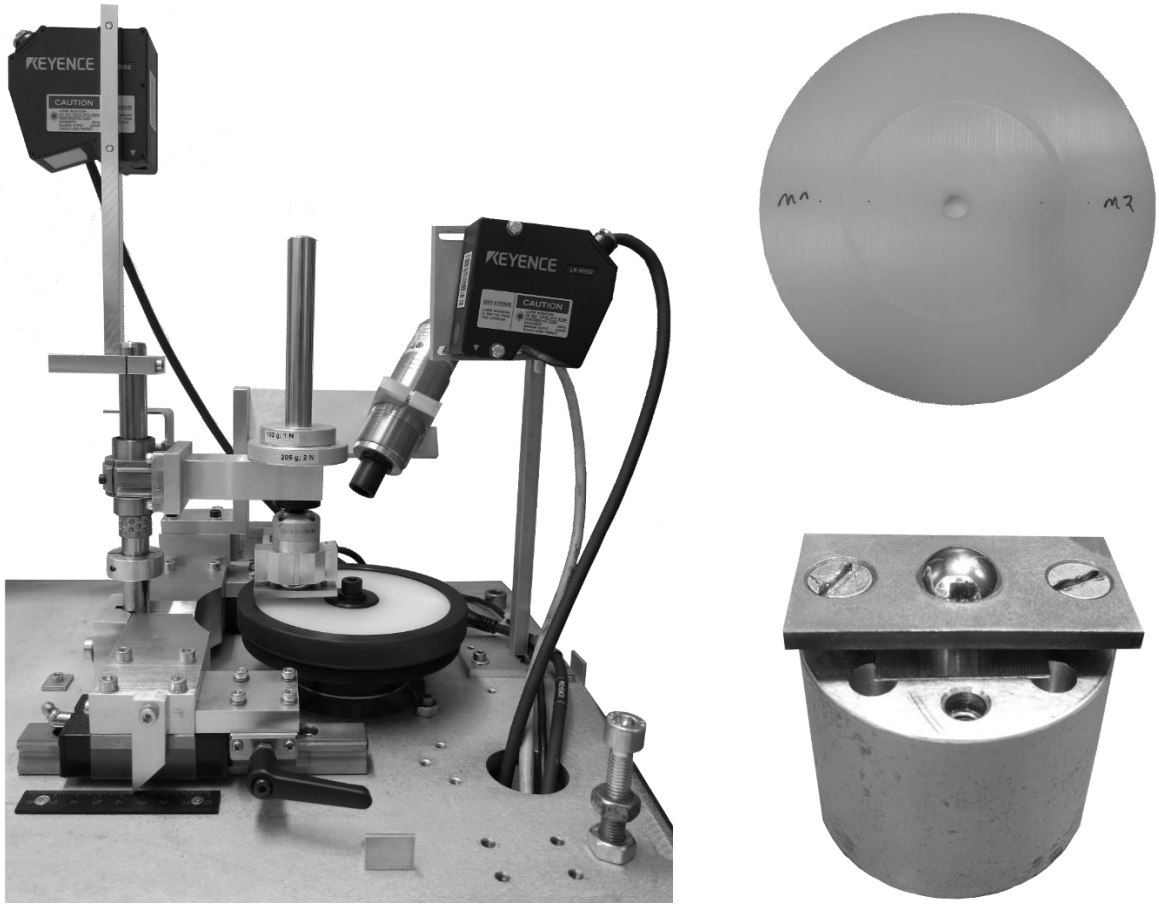

Figure 12: (left): ball on disc test machine including laser sensors (measurement of indentation depth) and pyrometer (temperature measurement); (right): PE-UHMW disc with running track (after test) and steel sphere in sample holder

To validate the analytical model (described in chapter 4) several tests are made with spheres from which a part has been removed via eroding (see Figure 13 left). These spheres are placed in the sample holder and the tilting angle can be adjusted with a self-constructed angle adjustment unit (Figure 13 middle).

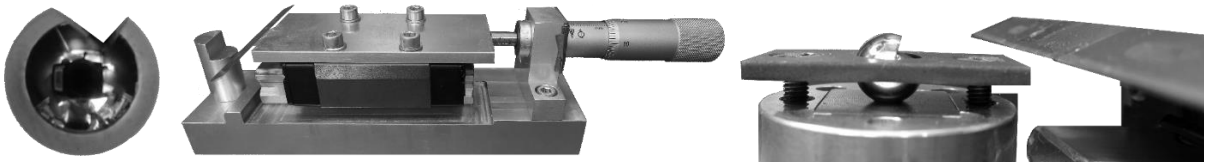

Figure 13: (left) steel sphere ø 8 mm with removed part; (middle): angle adjustment unit; (right): steel sphere ø 8 mm with removed part in sample holder after adjustment

On the left side of Figure 14 the assembly of the tilted "half-sphere" during a friction test is shown. On the right side the data of COF and indentation depth over a time period of 24 h is shown. For further calculation usually the averaged values between 21-23 h are considered.

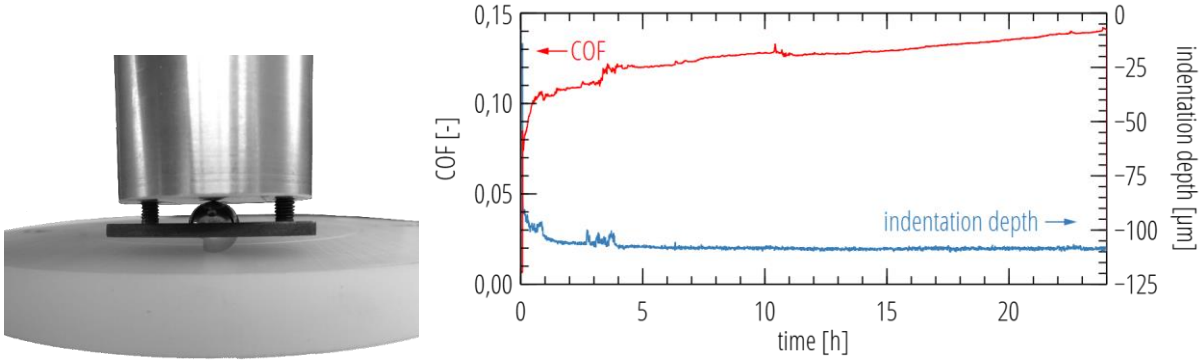

Figure 14: (left): tilted sphere during friction test; (right) measurement data of deformation and COF of PE-UHMW over 24 h

4. Analytical Model

The basic idea of calculating friction is described in [1] in detail. In summary, the calculation is based on Hertzian contact equations, which allow conclusions to be drawn about the real contact area by knowing the deformative part of friction. The approach according to [8], [9] and [10] forms the basis for the calculation of the contact area by introducing a rear angle ω.

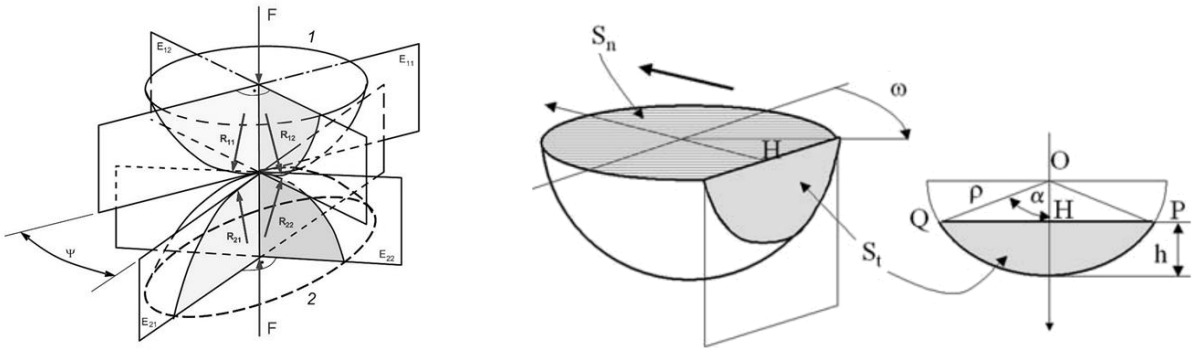

Figure 15: (left) static contact conditions of two bodies curved on all sites [11]; (right): definition of the resulting contact areas between a sphere and a plane counter body during movement with S_n normal section and S_t cross section (without contact) according [8]

In the present case, where a steel sphere is sliding over a polymer disc with normal forces from 10 to 150 N plastic deformation is present. This is expressed by a measurable running track which can be analysed after friction tests (Figure 16). The idea is that this cylindrically shaped running track forms the starting point for the calculation of the contact area and the deformative part of friction μ_{def}. From now on a Hertzian contact with the contact case *sphere in cylinder* (Polymer) is present. The radius of the cylinder

is the radius of the running track r_{track}. On the right side of Figure 16 the forming contact with Hertzian radius a is presented.

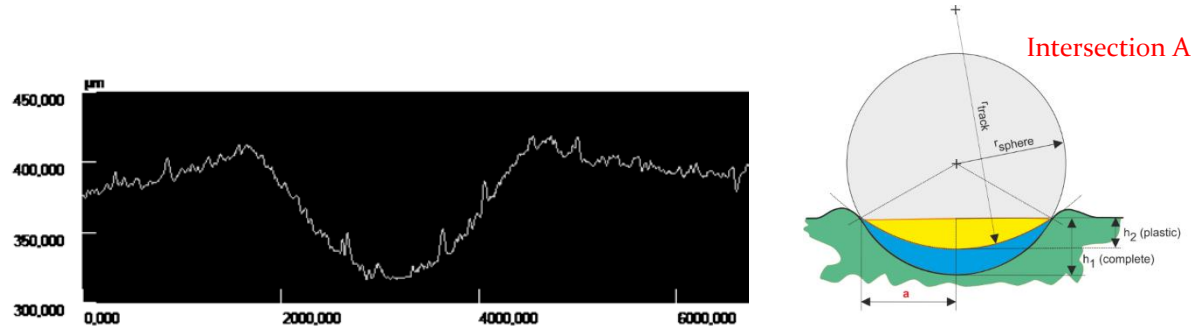

Figure 16: (left): profile of running track on PE-UHMW after 24 h friction test, measured with a laser scanning microscope; (right): intersection A (see Figure 17) with Hertzian contact radius a

Figure 17 shows the general shape of the forming contact zone when a sphere is moving over the cylindrical running track. While the front part with radiuses a and b_1 has a half elliptical shape, the rear part with radius a and b_2 forms an elliptical segment. Depending on the elastic (and viscoelastic) properties of the polymer b_2 can vary between 0 and b_1. These two cases can be interpreted as:

– $b_2 = 0$ fully plastic deformation and
– $b_2 = b_1$ fully elastic deformation

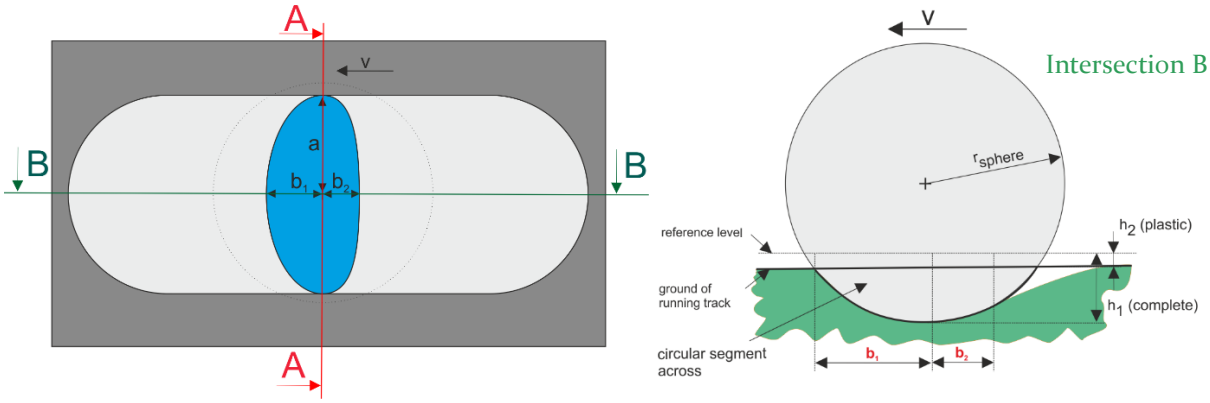

Figure 17: (left) running track (light grey) and forming contact area (blue) when a sphere is moving over the cylindrical shaped sample; (right): intersection B with resulting radii b_1 and b_2

To calculate the deformative part of friction the areas S_n and S_t need to be known (see Figure 15 right side) for the contact case of *sphere to cylinder*. The ratio of these two areas is defined as μ_{def}:

$$\mu_{def} = \frac{S_t}{S_n} \tag{1}$$

According to Figure 18 left the contact area can be described as an ellipsoid segment, where S_n is an ellipse (with radii a and b_1) with one part missing and S_t is a half ellipse (with radii $P(y)$ and z).

Calculation of S_n

For the calculation of S_n see Figure 18 right. The area of the full ellipse ($S_{ellipse}$), formed by a and b_1, and the area of the elliptical segment ($S_{ellipse,segment}$) must be subtracted from each other:

$$S_n(\omega) = S_{ellipse}(\omega) - S_{ellipse,segment}(\omega) \tag{2}$$

Therefor the points of intersection P_1 and P_2 of the ellipse $g(x)$ and $f(x)$ need to be calculated, while $f(x)$ depends on the rear angle ω:

$$f(x) = m * x, \; with\, m = \tan(\omega) \tag{3}$$

$$g(x) = \sqrt{{b_1}^2 - \frac{x^2 * {b_1}^2}{a^2}} \tag{4}$$

Equating $f(x)$ and $g(x)$ results in the points of intersection:

$$f(x) = g(x) \rightarrow P(x(\omega)) = \sqrt{\frac{{b_1}^2}{\tan(\omega)^2 + \frac{{b_1}^2}{a^2}}} \tag{5}$$

By knowing $P(x(\omega))$, $P(y(\omega))$ can be calculated:

$$P(y(\omega)) = \frac{b_1}{a}\sqrt{a^2 - P(x(\omega))^2} \tag{6}$$

With these points the area $S_{ellipse,segment}(\omega)$ can be calculated:

$$S_{ellipse,segment}(\omega) = a * b_1 * \arccos\frac{P(x(\omega))}{a} - P\big(x(\omega)\big) * P(y(\omega)) \tag{7}$$

Now the area $S_n(\omega)$ can be calculated:

$$S_n(\omega) = \pi * a * b_1 - a * b_1 * \arccos\frac{P(x(\omega))}{a} - P\big(x(\omega)\big) * P(y(\omega)) \tag{8}$$

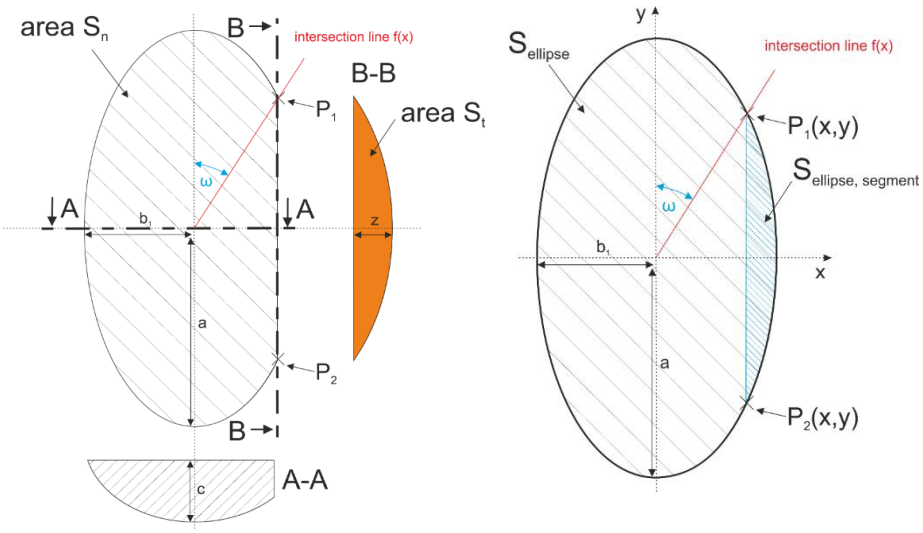

Figure 18: (left): contact area S_n and S_t with rear angle ω; (right): area $S_{ellipse}$ and $S_{ellipse,segment}$ calculation of S_n

Calculation of S_t

As mentioned earlier, the area S_t is a half ellipse with radii $P(y)$ and $P(z)$, while $P(z)$ can be calculated using the equation for an ellipsoid:

$$\frac{P(x)^2}{a^2} + \frac{P(y)^2}{{b_1}^2} + \frac{P(z)^2}{c^2} - 1 \tag{9}$$

With $P(x) = 0$ it follows:

$$P(z) = \sqrt{1 - \frac{P(y)^2}{{b_1}^2} * c^2} \tag{10}$$

c is the indentation depth (only the elastic part), which is determined by subtracting the indentation depth during the friction test (h_1) and the resulting plastic deformation (h_2), measured with a laser scanning microscope shown in Figure 17.

The area S_t can now be calculated:

$$S_t(\omega) = \frac{\pi * P(y(\omega)) * P(z(\omega))}{2} \tag{11}$$

By knowing S_t and S_n the deformative part of friction μ_{def} can be calculated.

$$\mu_{def}(\omega) = \frac{S_t(\omega)}{S_n(\omega)} = \frac{\pi * P(y(\omega)) * P(z(\omega))}{2\left(\pi * a * b_1 - a * b_1 * \arccos\frac{P(x(\omega))}{a} - P(x(\omega)) * P(y(\omega))\right)} \tag{12}$$

Following chart (Figure 19) shows the relation of μ_{def} and the rear angle ω depending on the normal force. The calculated results base on the real measurement data of indentation depth (h_1), the resulting plastic deformation (h_2) and the radius of the running track r_{track}. The main conclusion is, that the smaller the rear angle ω, the larger μ_{def}.

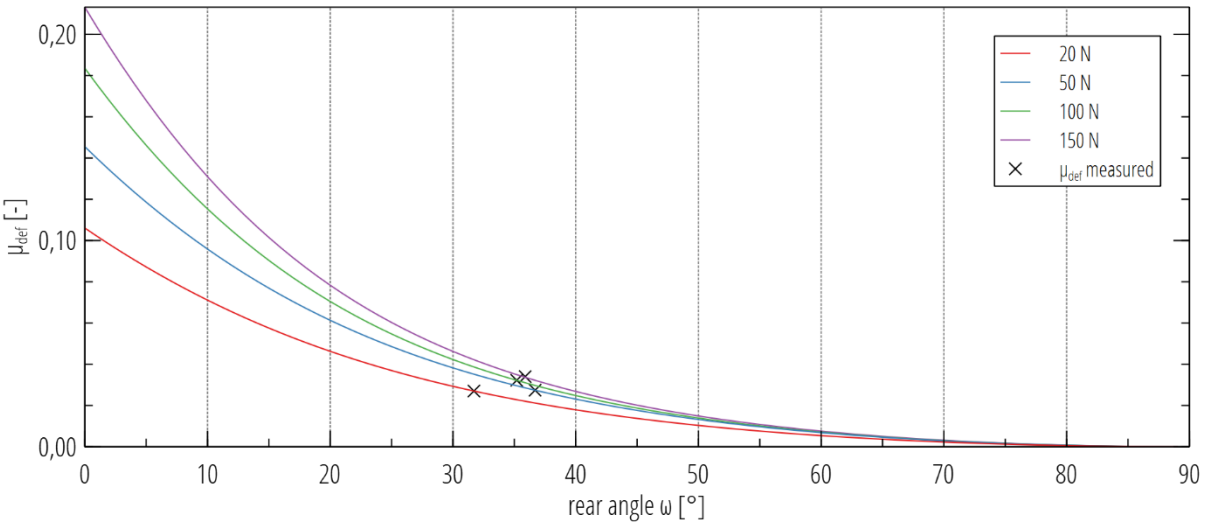

Figure 19: calculated rear angle ω depending on μ_{def} for different normal forces with measurement results of μ_{def}

From here on the only missing element in eq. 12 is μ_{def} which can be measured with lubricated sliding experiments as described in [12]. Figure 20 shows the comparison

between dry and lubricated friction measurements. The values of the lubricated experiments can be interpreted as μ_{def} due to missing adhesion by separating the two bodies with silicon oil. In summary, the deformative friction component μ_{def} accounts for about 1/4 and the adhesive friction component μ_{adh} for about 3/4 of the total friction μ_{total}.

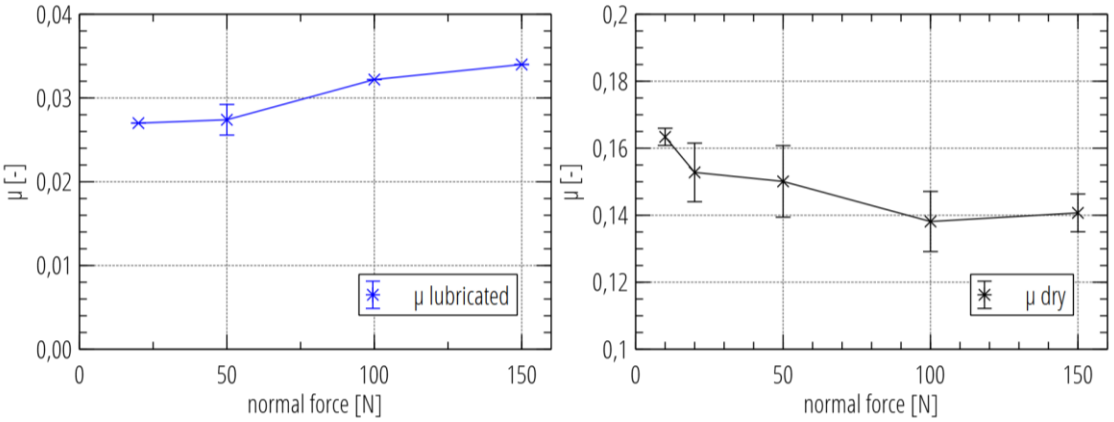

Figure 20: measurement data for μ depending on the normal force; (left): lubricated (with silicon oil) experiments; (right): dry experiments (Attention: different scales)

Based on the measured values of μ_{def} for each normal force the rear angle ω can now be calculated using equation 12. These values are marked with a cross in Figure 19 and lie between an angle 31,7° – 36,7°. In order to carry out the calculations the indentation depth is of great importance because it defines the Hertzian contact conditions. Therefor Figure 21 shows the comparison of the indentation depth h_1 (measured with the ball on disc test machine) for dry and lubricated experiments at a normal force of 50 N. The plotted data consist of 8 dry and 8 lubricated experiments and the mean values of $h_{1,dry,20-22h} = 107{,}5 \pm 6\ \mu m$ and $h_{1,lubricated,20-22h} = 108{,}8 \pm 1{,}6\ \mu m$ are close together and have a low scattering. The very low scattering of the lubricated experiments can be explained be less influence of surface interaction of the specimen due to absence of adhesion.

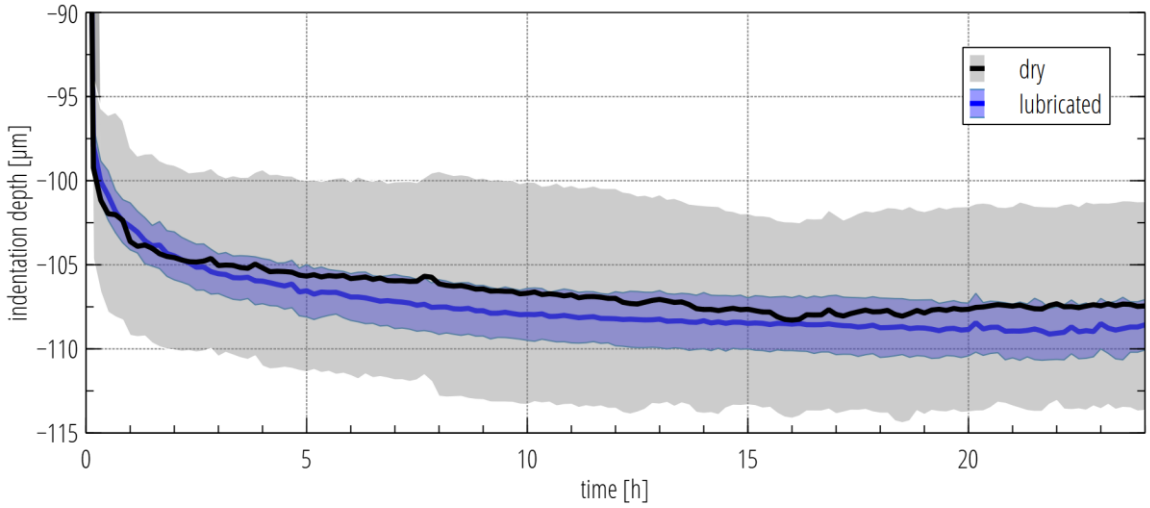

Figure 21: comparison of indentation depth h_1 over time for dry and lubricated friction tests (mean values of 8 tests each, F_N = 50 N)

To verify the accuracy of the analytical calculation model, another set of experiments was necessary. Therefore, as described in chapter 3.4, spheres with removed part with enables a partial contact at the backside are used. The tilting angle can now be adjusted until the indentation depth h_1 equals the results of the "full sphere". The idea is that if the tilted angle of the "half sphere" is smaller than the correct rear angle ω, the sphere will penetrate deeper into the material as long as the area is similar to that of the "full sphere".

Figure 22 shows the results of the tests with F_N = 20 N for PE-UHMW under variation of the rear angle ω. The reference value of the indentation depth is given by the results of the "full sphere". If the "half sphere" is tilted too far (15,16 and 25,2°) the indentation depth increases. The best result is reached with a "half sphere" with an adjusted rear angle ω = 41,5°. The calculated rear angle ω (with equation 12) is 31,7°.

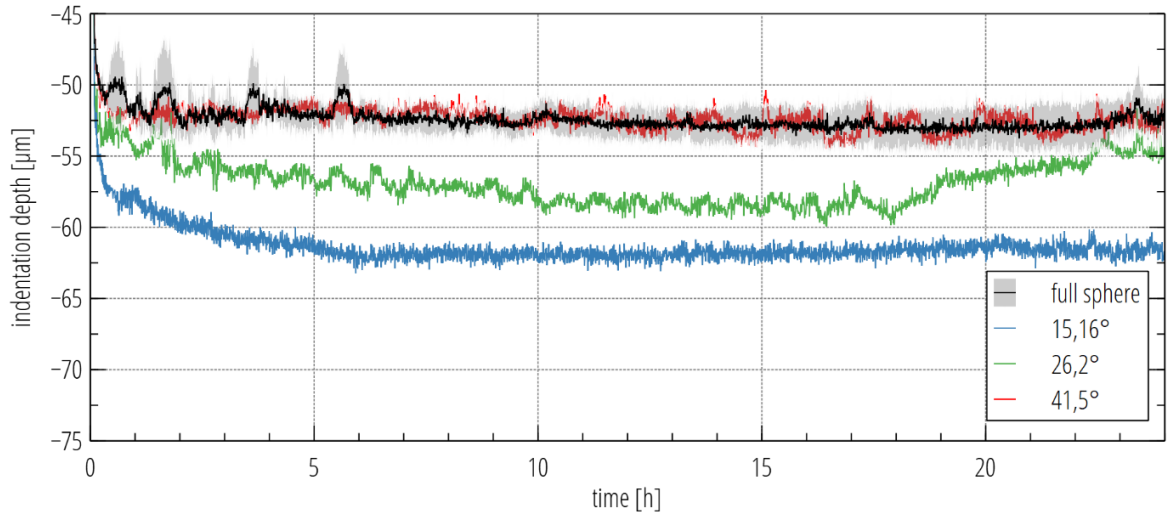

Figure 22: indentation depth h_1 for F_N = 20 N over time for dry friction tests with different rear angle ω

The same method was applied to the other normal loads. For F_N = 50 N an adjusted rear angle ω = 36,97° fitted best, while the calculated rear angle ω is 36,69° (Figure 23).

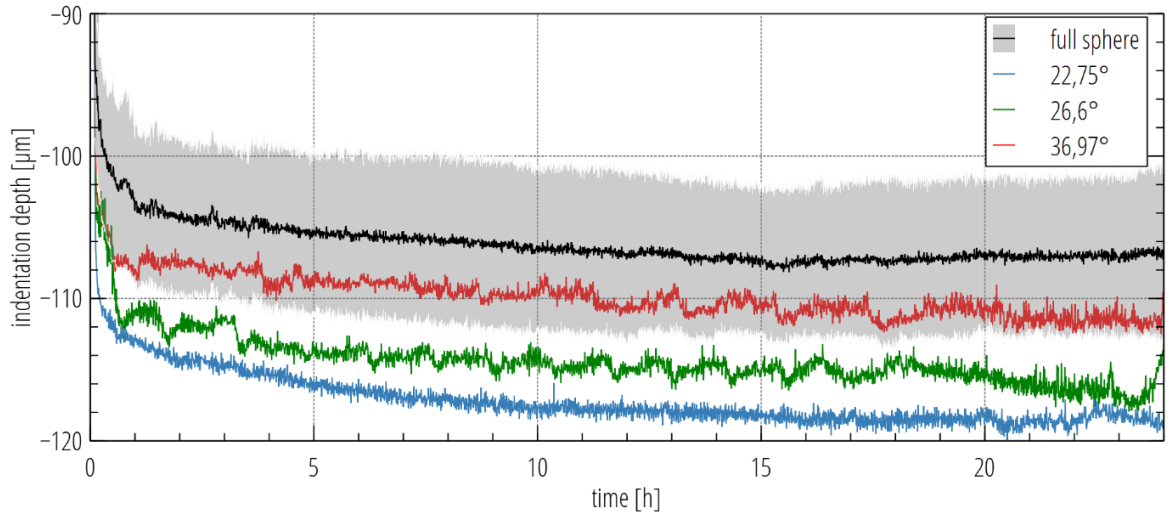

Figure 23: indentation depth h_1 for F_N = 50 N over time for dry friction tests with different rear angle ω

For F_N = 100 N an adjusted rear angle ω = 36,48° fitted best, while the calculated rear angle ω is 35,2° (Figure 24).

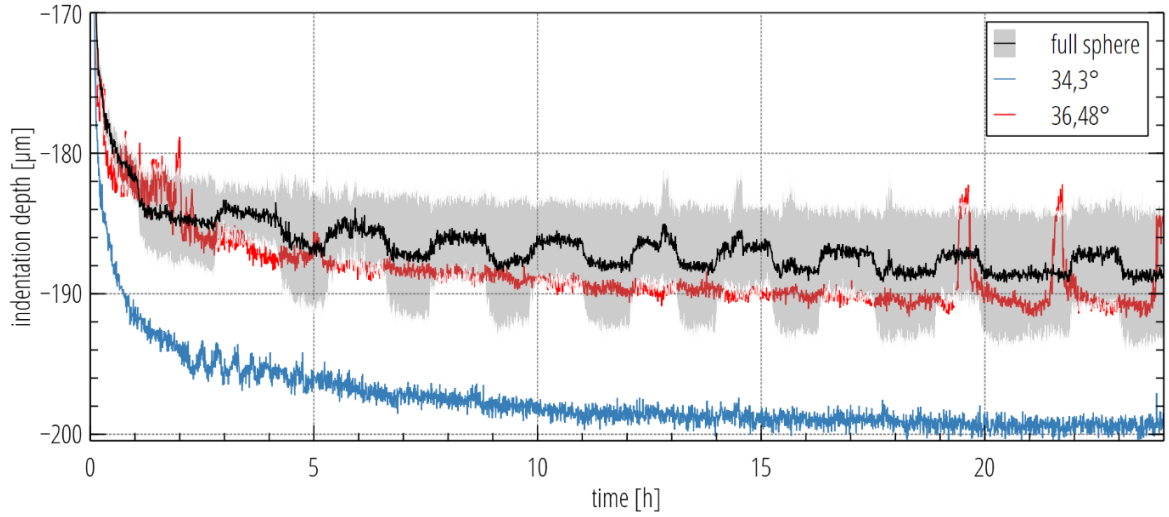

Figure 24: indentation depth h_1 for F_N = 100 N over time for dry friction tests with different rear angle ω

For F_N = 150 N an adjusted rear angle ω = 66,82° fitted best, while the calculated rear angle ω is 35,9° (Figure 25).

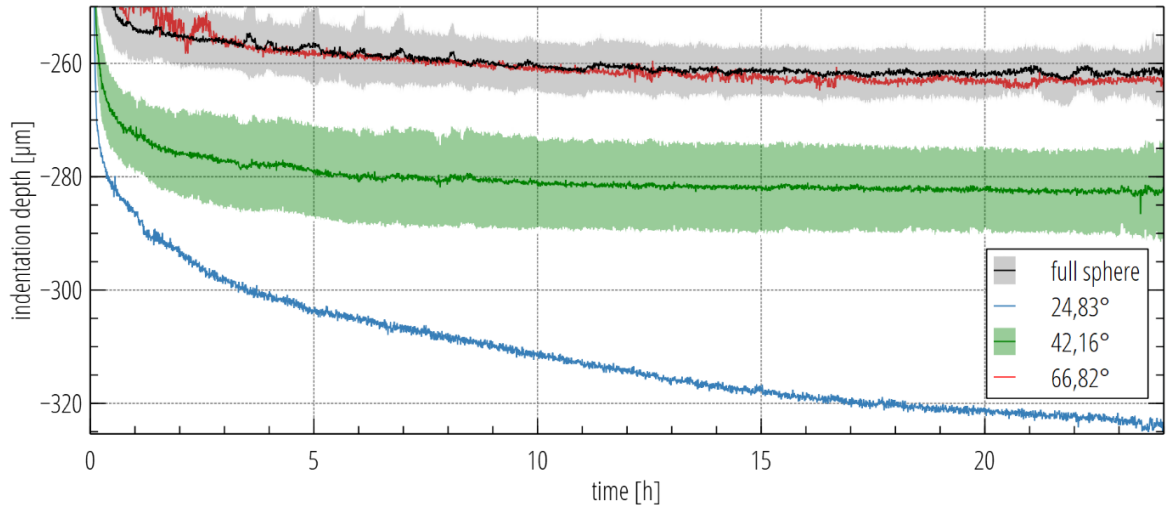

Figure 25: indentation depth h_1 for F_N = 150 N over time for dry friction tests with different rear angle ω

Table 2 gives an overview of the deviation of the experimentally measured and the calculated rear angle ω. While for F_N = 50 and 100 N the deviation is very small, especially for F_N = 150 N it is significant. The deviation of 30 % for F_N = 20 N may be caused by inaccurate geometry data of the running track due to very small plastic deformations after the friction tests. The radius r_{track} and the plastic deformation h_2 define the Hertzian contact and minor deviations can lead to major differences in the rear angle ω. For F_N = 150 N more tests are planned to study the behaviour in detail.

Table 2: comparison of the experimentally measured and the calculated rear angle ω

normal load [N]	calculated rear angle ω [°] (using equation 12)	measured rear angle ω [°]	deviation [%]
20	31,7	41,5	+30
50	36,69	36,97	+0,7
100	35,2	36,48	+3,6
150	35,9	66,82	+86

5. FEM Simulation

The FEM-based parametric studies of the complex friction processes in the contact case sphere versus plane require material models of the raw materials that are as accurate as possible. Concerning the planned investigations on multiple contacts between structured and smooth plastic surfaces of different materials (POM versus PE-UHMW), strongly deviating material models would potentiate the errors.

Utilizing the software MCalibration® and the results of various calibration experiments, the parameters of the rheological material models are optimized accordingly. The calibration tests include tensile tests (section 3.1) and compression tests (section 3.2). The instrumented indentation tests (section 3.3) serve as validation test for the quality of the calibration with regard to the later complex friction simulations.

Figure 26 shows the comparison between the measured values of the instrumented indentation tests compared to the results of the FEM simulations. The total displacement (indentation depth) of the spherical indenter in relation to the normal force, serves as an evaluation criterion.

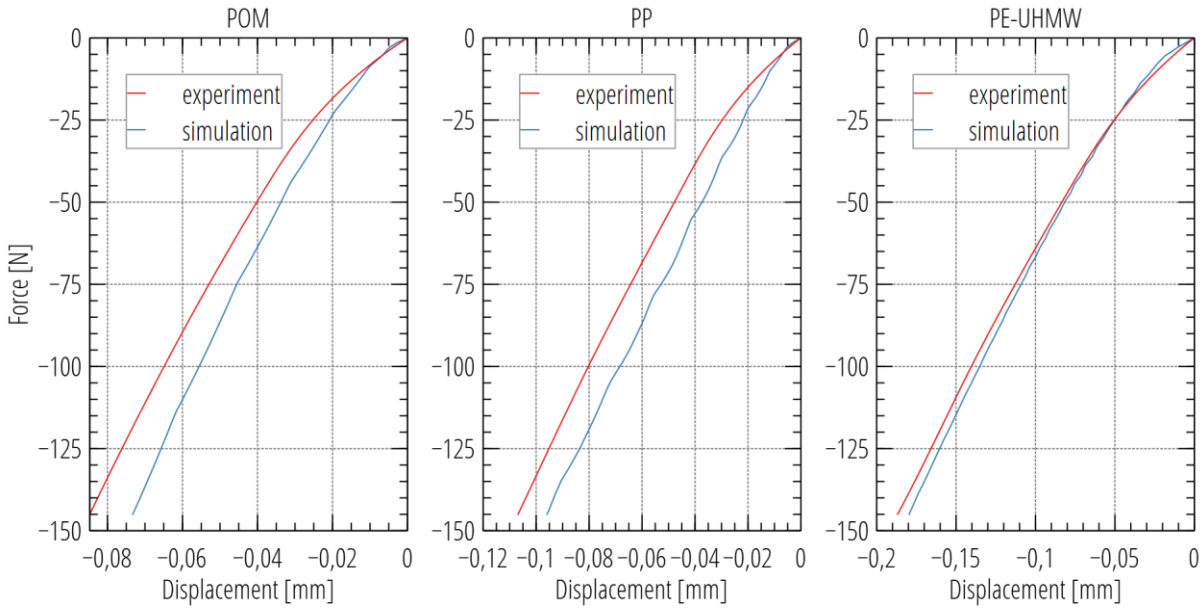

Figure 26: comparison between the measured values of the instrumented indentation tests (experiment) and the FEM simulations (simulation) using the calibrated material model for the respective material

For the materials PP and PE-UHMW the Abaqus® native model PRF-3YP (Parallel Rheological Framework-3 Yeoh Networks with Power-Law Flow) was used. This model delivered the best results in the optimization runs. In the case of POM the Three Network (TN) model [13] was used. The TN model is part of the external material library PolyUMod®.

The deviations between the instrumented indentation tests and the FEM simulations are shown in Table 3 for each material. In general, the calibrated material models show a stiffer behaviour than the real materials.

Table 3: percentage deviations between final values of the indentation tests and the FEM simulations

material	**normal force [N]**	**measured ind. depth [mm]**	**simulated ind. depth [mm]**	**deviation [%]**
POM	-142	-0,0835	-0,0721	-13,7
PP	-143,5	-0,1060	-0,0951	-10,3
PE-UHMW	-145	-0,1868	-0,1795	-3,9

The measured values used for the calibration of the material models should always correspond to the experimental parameters of the later simulation parameters. This concerns e. g. the compressive or tensile load as well as the loading velocities. In the further progress of the research, adjustments regarding the material models will have to be made, which consider these influences.

6. Conclusion and Outlook

This paper presents two different approaches to the calculation of the coefficients of friction. The work aims to determine the contact processes on single contacts and transfer them subsequent to more complex multiple contact situations.

A calculation approach for determining the deformative part of COF was demonstrated based on the analytical calculation model and validated with experiments. By varying the rear angle behind the sphere (area without contact) it could be demonstrated that the indentation depth and finally the contact area are closely connected and can be used to describe the deformative part of COF. For some load cases (F_N = 50 and 100 N), the deviation between calculation and experiments was negligible. The load cases F_N = 20 and 150 N require additional tests. Further steps include the development of calculation approaches for the adhesive part of COF and to transfer the results to multiple contacts.

The state of the FEM simulation is, that a set of calibrated material models for POM, PP, and PE-UHMW exist. They were validated with instrumented indentation tests. The deviation ranges here between 4 -14 %. Furthermore, an extensive database of dynamic and quasi-static tensile and compression tests is available for future material model adaptations. These material models provide a starting point for creating more-complex FEM models to study the friction processes between smooth and textured thermoplastic specimen. The following steps of FEM modelling concern the mapping of long-term

friction tests of spherical indenters (steel and thermoplastic) on a thermoplastic plane. This step requires the extension of the material models concerning their viscous deformation components and creep properties. The overall aim is to investigate the influence of macroscopic surface structures on the frictional properties of thermoplastic materials with the help of FEM models.

Acknowledgement

The research project was funded by the Federal Ministry of Economic Affairs and Energy (BMWi) through the "Otto von Guericke" German Federation of Industrial Research Associations (AiF) on the basis of a resolution of the German Bundestag as part of the programme to promote joint industrial research (IGF No. 20967 BG).

References

[1] Bergmann, A, et al.: "Calculation Approaches for Determining the Sliding Friction Coefficient – Analytical Consideration and FE-Modelling", innoTRAC, vol. 1, pp. 95–106, Dec. 2020. DOI: 10.14464/innotrac.v1i0.460

[2] https://www.roechling.com/de/industrial/werkstoffe/thermoplastische-kunststoffe/detail/polystone-m-natur-72, website visited 03.09.2021

[3] https://tools.celanese.com/products/datasheet/SI/HOSTAFORM%C2%AE%20C%209021, website visited 03.09.2021

[4] https://www.campusplastics.com/material/pdf/141226/POLYFORTFPP22TLEK1684 ?sLg=de&layout=automotiveoempdf&ci=4, website visited 03.09.2021

[5] https://silikon-profis.de/ELBESIL-SILIKONOeL-B-50-50-cSt-im-500-g-oder-10-kg-Gebinde, website visited 03.09.2021

[6] DIN EN ISO 604, Kunststoffe Bestimmung von Druckeigenschaften (ISO 604:2002); Deutsche Fassung EN ISO 604:2003

[7] Bergström, J.: Can Friction Cause Viscoelasticity? https://polymerfem.com/can-friction-cause-viscoelasticity/, website visited 03.09.2021

[8] Lafaye, S., et al.: The ploughing friction Analytical model with elastic recovery for a conical tip with a blunted spherical extremity, Tribology Letters, Vol. 21, No. 2:95-99 (2006)

[9] Lafaye, S., et al.: Analyzing friction and scratch tests without in situ observation, Wear 265: 664–673 (2008)

[10] Goddard, J., et al.: A Theory of Friction and Wear during the Abrasion of Metals, Wear 5:114-135 (1962)

[11] Kunz, J.: Kontaktprobleme und ihre praktische Loesung, Konstruktion 11/12 2009, VDI Verlag (2009)

[12] Rodriguez, P.: Contact and Friction in Systems with Fibre Reinforced Elastomers; Dissertation (2012)

[13] Bergström, J., Bischoff, J.: An advanced thermomechanical constitutive model for UHMWPE. International Journal of Structural Changes in Solids. 2. 31-39 (2010)